BMP signaling maintains auricular chondrocyte identity and prevents microtia development by inhibiting protein kinase A

Ruichen Yang[1*], Hongshang Chu[1*], Hua Yue[2], Yuji Mishina[3], Zhenlin Zhang[2], Huijuan Liu[1,5], and Baojie Li[1,4,5]

[1]Bio-X Institutes, Key Laboratory for the Genetics of Developmental and Neuropsychiatric Disorders, Ministry of Education, Shanghai Jiao Tong University, Shanghai, China.

[2]Department of Osteoporosis and Bone Diseases, Shanghai Clinical Research Center of Bone Disease, Shanghai Jiao Tong University Affiliated Sixth People's Hospital, Shanghai, China.

[3]Department of Biologic and Materials & Prosthodontics, University of Michigan School of Dentistry, Ann Arbor, MI, United States.

[4]Institute of Traditional Chinese Medicine and Stem Cell Research, Chengdu University of Traditional Chinese Medicine, Chengdu, China.

* equal contribution

[5] Correspondence:
Baojie Li: libj@sjtu.edu.cn

Or

Huijuan Liu liuhj@sjtu.edu.cn

Abstract

Elastic cartilage constitutes a major component of the external ear, which functions to guide sound to the middle and inner ears. Defects in auricle development cause congenital microtia, which affects hearing and appearance in patients. Mutations in several genes have been implicated in microtia development, yet, the pathogenesis of this disorder remains incompletely understood. Here, we show that *Prrx1* genetically marks auricular chondrocytes in adult mice. Interestingly, BMP-Smad1/5/9 signaling in chondrocytes is increasingly activated from the proximal to distal segments of the ear, which is associated with a decrease in chondrocyte regenerative activity. Ablation of *Bmpr1a* in auricular chondrocytes led to chondrocyte atrophy and microtia development at the distal part. Transcriptome analysis revealed that *Bmpr1a* deficiency caused a switch from the chondrogenic program to the osteogenic program, accompanied by enhanced protein kinase A activation, likely through increased expression of *Adcy5/8*. Inhibition of PKA blocked chondrocyte-to-osteoblast transformation and microtia development. Moreover, analysis of single-cell RNA-seq of human microtia samples uncovered enriched gene expression in the PKA pathway and chondrocyte-to-osteoblast transformation process. These findings suggest that auricle cartilage is actively maintained by BMP signaling, which maintains chondrocyte identity by suppressing osteogenic differentiation.

Introduction

The ear is an organ of hearing and equilibrium. The external ear (auricle), which contains many curves and folds, functions to collect and funnel sound waves into the middle and inner ear (Anthwal and Thompson, 2016; Fuchs and Tucker, 2015). The major component of the ear is elastic cartilage, a connective tissue composed of type II collagen, proteoglycans and glycosaminoglycans (Bielajew et al., 2020; Chen et al., 2021). Defects in auricle development can lead to microtia, a congenital disease characterized by deformed or underdeveloped ears that affects 0.83-4.34 per 10000 births (Gendron et al., 2016; Lu et al., 2020). Microtia causes hearing problems and delays in language learning (Gendron et al., 2016). Genetic studies have shown that microtia is linked to mutations in *ROBO1/ROBO2*, *HOXA2*, *SIX*, *TBX1*, or *CHUK* in humans (Cox et al., 2014; Huang et al., 2023; Lu et al., 2020; Quiat et al., 2022). In mice, Prrx1 and Prrx2, FGF, BMP, and Wnt have been shown to affect auricle development (ten Berge et al., 1998; Xie et al., 2020). However, the molecular etiology of microtia remains incompletely understood. Currently, microtia is treated with ear reconstruction (Evenbratt et al., 2022; Kobayashi et al., 2011; Nordberg et al., 2022).

Cartilage is an avascular and slow-turnover tissue that receives nutrients and external signals via diffusion (DiDomenico et al., 2018). In addition to elastic cartilage, hyaline cartilage and fibrocartilage are found in mammals. Cartilage is located in different parts of the body and has several important functions, including support, protection, and cushioning (Bielajew et al., 2020; Liu et al., 2017). Elastic cartilage is found in the ear, epiglottis, nose, and trachea, and its main function is to provide strength and elasticity to the organs. All cartilages are formed and maintained solely by chondrocytes (Kozhemyakina et al., 2015). Chondrocytes are extensively studied in endochondral ossification, which forms long bones. Bone development starts with condensation of mesenchymal cells, which differentiate into chondrocytes and form a cartilage template for the bones. After proliferation, differentiation, and hypertrophic growth, hypertrophic chondrocytes undergo transformation into osteoblast/osteoprogenitors (transdifferentiation or dedifferentiation followed by

68 redifferentiation), forming bone (Jing et al., 2017; Mizuhashi et al., 2018; Newton et
69 al., 2019; Yang et al., 2014a; Yang et al., 2014b). On the other hand, auricle
70 chondrocytes are derived from pharyngeal arches 1 and 2 during development (Ritter
71 and Martin, 2019). Although the auricle contains $CD44^{+}CD90^{+}$ stem cells in the
72 perichondrium (Kobayashi et al., 2011), it has limited regenerative capacity even in
73 early postnatal mice (Abarca-Buis and Krotzsch, 2023).

74 Chondrocyte proliferation, differentiation, and hypertrophy are regulated by BMPs,
75 FGFs, IHHs, PTHrp, and Wnts. In particular, BMP signaling positively regulates the
76 initiation and differentiation of chondrocytes (Murtaugh et al., 1999; Thielen et al.,
77 2019; Ueharu and Mishina, 2023). BMPs are members of the TGFβ superfamily, which
78 bind to BMP receptor IA and IB and activate Smad1/5/9, which, together with Smad4,
79 enter the nucleus to affect gene expression. *Bmpr1a* and *1b* double knockout mice have
80 no chondrocyte formation (Yoon et al., 2005). Moreover, ablation of *Smad1* or *Smad5*
81 in chondrocytes leads to severe chondrodysplasia (Retting et al., 2009), indicating that
82 BMP signaling is essential for maintenance of the chondrogenic differentiation program.
83 In addition, chondrocyte-specific knockout of *Bmpr1a* and *Bmpr1b* resulted in defects
84 in the terminal differentiation of chondrocytes (Yoon et al., 2006). BMPs induce
85 chondrocyte differentiation by controlling the expression of Sox9, which initiates and
86 maintains the chondrocyte phenotype but inhibits chondrocyte hypertrophy (Akiyama
87 et al., 2002). Sox9 may interact with Runx2 and β-catenin to regulate chondrocyte
88 differentiation and hypertrophy (Kozhemyakina et al., 2015; Takarada et al., 2013). A
89 recent study showed that *Sox9* is required to prevent growth plate closure postnatally,
90 with Sox9 ablation leading to transformation from chondrocytes to osteoprogenitor
91 cells (Haseeb et al., 2021).

92 Here, we provide genetic evidence that BMP signaling maintains the cell fate of
93 auricle chondrocytes. In the absence of BMP signaling, chondrocytes become
94 osteogenic progenitors with reduced volume, leading to shrinkage of the distal auricle
95 and morphological changes that resemble microtia. This study uncovered a new

96 function for BMP signaling and improved our understanding of the pathogenesis of
97 microtia.

Results

Prrx1 marks auricle chondrocytes but few epiphyseal or articular chondrocytes

We have recently shown that *Prrx1* marks $CD31^{-}CD45^{-}CD130^{+}CD200^{+}CD51^{+}$ skeletal stem cells that are required for bone maintenance in adult mice (Liu et al., 2022). Our lineage tracing experiments showed that *Prrx1* marked all chondrocytes in the auricle (Fig. 1A). This finding is in contrast to the labeling of very small populations of chondrocytes in the growth plates and articular cartilages (Fig. 1B). As expected, *Prrx1* also marked dermal cells in the skin of the ear (Fig. 1A); we previously showed that *Prrx1* marks $CD31^{-}CD45^{-}CD200^{+}CD51^{+}$ dermal stem cells (Liu et al., 2022). Immunostaining results showed that auricle chondrocytes did not express Vimentin or Col1α1/2, which were mainly expressed in the dermis of the ear, or Col2 or Col10 (Fig. 1C and data not shown). Moreover, αSMA is mainly expressed in the smooth muscle of blood vessels (Fig. 1C). These results suggest a difference between auricle cartilage and articular cartilage and growth plates.

Ablation of *Bmpr1a* in *Prrx1*$^{+}$ cells in adult mice led to microtia

We generated *Prrx1-CreERT; Bmpr1a*$^{f/f}$ mice to study the function of BMP signaling in adult cartilage. TAM was injected at 12 weeks of age. We observed a decrease in p-Smad1/5/9 on the ear sections of the *Prrx1-CreERT; Bmpr1a*$^{f/f}$ mice 60 days after TAM administration (Fig. 2A). qPCR analysis confirmed the ablation of *Bmpr1a* in the auricle cartilage (Fig. 2B). Note that the size and body weight of *Prrx1-CreERT; Bmpr1a*$^{f/f}$ mice were slightly reduced (Supplementary Fig. S1A). Interestingly, the mice showed a quick decrease in the size of the external ear (Fig. 2C), indicating a problem with auricle cartilage, which provides strength for the ear.

Histological analysis showed that the phenotype mainly occurred at the distal part of the ear. The thickness of the cartilage was slightly reduced, associated with a great reduction in the cell size (Fig. 2D). Staining for Ki67 showed that there was no difference in the number of proliferating cells between the mutant and control mice (Supplementary Fig. S1B). Staining for apoptotic cells indicated that chondrocytes did not undergo apoptosis (Supplementary Fig. S1C). Overall, these results suggest that the ear phenotype observed in *Prrx1-CreERT; Bmpr1a*$^{f/f}$ mice is not due to changes in chondrocyte proliferation or apoptosis; rather, it occurs through shrinkage of chondrocytes. Interestingly, deletion of both *Prrx1* and *Prrx2* also led to microtia development (ten Berge et al., 1998), suggesting that these two genes play a role in

elastic chondrocytes. However, we found no ear phenotype in *Prrx1-CreERT* (with one *Prrx1* allele deleted) or *Bmpr1a*$^{f/f}$ mice compared to wild-type mice (Supplementary Figs. S2A and S2B), suggesting that ablation of one copy of *Prrx1* does not affect ear maintenance.

The growth plate and the articular cartilage appeared to be normal in *Prrx1-CreERT; Bmpr1a*$^{f/f}$ mice (Supplementary Figs. S3A and S3B), likely due to the lack of labeling of chondrocytes at these locations. Moreover, Smad1/5/9 is reportedly activated in proliferating chondrocytes but not hypertrophic chondrocytes in the growth plate (Retting et al., 2009; Yoon et al., 2006).

Ablation of *Bmpr1a* in *Prrx1*$^{+}$ cells in young mice also led to microtia

We then tested the effect of *Bmpr1a* ablation on *Prrx1*$^{+}$ cells in young mice. Three doses of TAM were administered to P21 *Prrx1-CreERT; Bmpr1a*$^{f/f}$ mice, which were sacrificed at the age of 2 months (Fig. 3A). We observed a decrease in p-Smad1/5/9 on the ear sections of the *Prrx1-CreERT; Bmpr1a*$^{f/f}$ mice (Fig. 3A). qPCR analysis confirmed the ablation of *Bmpr1a* in the auricle cartilage (Fig. 3B). We found decreases in the ear size and the volumes of chondrocytes at the distal part of the ear in *Prrx1-CreERT; Bmpr1a*$^{f/f}$ mice (Figs. 3C and 3D). However, these mice showed normal growth plates and articular cartilage (Supplementary Figs. S4A and S4B), likely attributable to the lack of labeling of chondrocytes in the growth plate and articular cartilage in *Prrx1-CreERT; R26*^{tdTomato} mice. Overall, these results suggest that BMP signaling is required for both growth and maintenance of the auricle.

Chondrocytes in the distal auricle have the weakest regenerative ability

A surprising finding is that the auricle phenotype mainly occurred in the distal part (Figs. 2D and 3D), suggesting that there exists a cellular difference along the proximal–distal axis. Our immunostaining of p-Smad1/5/9 results revealed that BMP-Smad1/5/9 signaling is more active at the distal part than at the proximal or middle part, in young or adult mice (Fig. 2A and supplementary Fig. S5A). We also harvested cartilage from the proximal, mid, and distal (1/3 each) parts of normal adult mice and performed western blotting. We found that BMP-Smad1/5/9 signaling was activated to a greater extent at the distal part of the auricle (Supplementary Fig. S5B).

We then tested the regenerative potential of the proximal, mid, and distal parts of the auricle by performing cartilage regeneration assays. We generated a 0.2 cm hole at

these three locations and waited for 4 weeks. It was clear that the injury at the distal or middle part could not be repaired, while the injury at the proximal part was repaired (Supplementary Figs. S5C and S5D). These results suggest that chondrocytes at the distal part of the auricle have the lowest regenerative activity and thus may be the most differentiated, which is associated with the strongest activation of BMP-Smad1/5/9 signaling.

Ablation of *Bmpr1a* in dermal cells did not cause microtia

Since *Prrx1* also marks dermal cells in the ear, we could not exclude the possibility that *Bmpr1a* ablation in dermal cells contributes to the ear phenotype. We found that *Col1a2* marked dermal cells but not auricle chondrocytes in *Col1a2-CreERT; R26*^{tdTomato} mice (Supplementary Fig. S6A). We generated *Col1a2-CreERT; Bmpr1a*$^{f/f}$ mice by crossing *Prrx1-CreERT* mice and *Bmpr1a* floxed mice. Immunostaining results showed that the levels of p-Smad1/5/9 in the dermis were greatly reduced in dermal cells in the mutant mice (Supplementary Fig. S6B). qPCR analysis confirmed the ablation of *Bmpr1a* in the dermal cells (Supplementary Fig. S6C). The ears appeared normal in *Col1a2-CreERT; Bmpr1a*$^{f/f}$ mice 6 months after TAM injection (Supplementary Fig. S6D and S6E).

In addition, we traced the Acta2 (encoding αSMA) lineage cells in auricles and found that Acta2 could mark a small portion of chondrocytes in the middle segment of the auricle and smooth muscle cells of the blood vessels (Supplementary Fig. S7A). We also generated *Acta2-CreERT; Bmpr1a*$^{f/f}$ mice and found that ablation of *Bmpr1a* in *Acta2*$^{+}$ cells did not produce an ear phenotype (Supplementary Figs. S7B-S7E). These findings suggest that BMP-Smad1/5/9 signaling affects ear maintenance via its effect on chondrocytes at the distal segment, with little contribution from dermal cells or smooth muscle cells.

Alteration of transcription profiles in *Bmpr1a*-deficient chondrocytes

We then harvested the distal part of the auricle from three *Prrx1-CreERT; Bmpr1a*$^{f/f}$ and age- and gender-matched control mice. We prepared the total RNA and performed bulk RNA-seq. We found that the transcription of at least 500 genes was affected by *Bmpr1a* ablation (Fig. 4A). KEGG and GO analyses revealed that *Bmpr1a* ablation led to increased expression of genes in inflammation, stemness, cell cycle, mesenchymal cell development, proximal/distal patterning, ear morphogenesis, wound healing, TGFβ signaling, and PKA signaling, whereas genes in chondrocyte differentiation, stem cell

division, skeletal morphogenesis, cartilage development, Hedgehog signaling, and Wnt signaling were suppressed (Figs
. 4B and 4C). These transcriptome results suggest that *Bmpr1a* ablation may cause chondrocyte-to-osteoblast transformation.

Bmpr1a deficiency leads to an auricle chondrocyte switch to osteoblasts

The heatmaps of osteoblast-related and chondrocyte-related genes further support a chondrocyte-to-osteoblast transformation in the absence of BMP signaling (Fig. 5A and Supplementary Fig. S8A). To validate the above findings, we stained the auricle for Col1α1, a marker for osteoblasts, and found that Col1α1 expression was elevated in the auricle of the *Prrx1-CreERT; Bmpr1a*$^{f/f}$ mice compared to the control mice (Fig. 5B). We also stained for alkaline phosphatase (ALP), a marker for osteoblasts, and found that ALP activity was greatly increased in the mutant mice (Fig. 5C). WB confirmed the increases in the expression of osteoblast marker Runx2 and osteocalcin (Fig. 6D). These results suggest that in the absence of BMP signaling, auricle chondrocytes transformed into osteoblasts/osteoprogenitors via transdifferentiation or dedifferentiation/redifferentiation. Previous studies have shown that Sox9 is involved in chondrocyte to osteoblast transformation (Lefebvre et al., 2019). However, we found that Sox9 mRNA levels were not altered by *Bmpr1a* deficiency (Supplementary Fig. S8B and S8C).

Bmpr1a deficiency led to hyperactivation of the PKA pathway

To understand the molecular mechanisms underlying the development of microtia, we examined the signaling pathways altered by *Bmpr1a* deficiency in auricle samples. We focused on the enhanced activation of the protein kinase A pathway, which is known to regulate chondrocyte differentiation. PKA signaling has been shown to promote chondrocyte differentiation but inhibit chondrocyte hypertrophy (Dy et al., 2012; Tsang and Cheah, 2019). In addition, PKA-phosphorylated Sox9 (Huang et al., 2000) may promote bone formation (Siddappa et al., 2008). Immunoassaying for p-Creb, a substrate of PKA, suggests that PKA is activated in auricle chondrocytes compared to the control counterparts (Fig. 6A). Western blot analysis of the auricle samples confirmed this finding (Fig. 6B).

What caused the enhanced activation of the PKA pathway? Our RNA-seq data showed that the expression of Adcy5 and Adcy8 enzymes responsible for cAMP production, was upregulated in the *Bmpr1a*-deficient auricle samples. Our qPCR

analysis of auricle RNA showed that *Bmpr1a*-deficient auricle samples displayed increases in *Adcy5* and *Adcy8* (Fig. 6C).

Inhibition of PKA signaling blocks microtia development in *Bmpr1a*-deficient mice

To demonstrate the function of elevated PKA signaling in the development of microtia, we administered the PKA inhibitor H89 to *Prrx1-CreERT; Bmpr1a*$^{f/f}$ and control mice immediately after TAM injection (Fig. 7A). After 2 months, we found that p-Creb was greatly suppressed and that the microtia phenotype was rescued in the mutant mice by H89, although the inhibitor did not affect the auricle in the normal mice (Fig. 7B and 7C). Histological analysis revealed that chondrocyte atrophy and the decrease in ear size and cartilage thickness were rescued by H89 (Fig. 7D). Staining results revealed that the levels of Col1α1 and the ALP activity returned to normal (Fig. 7E and 7F). Western blot analysis of the auricle samples confirmed that inhibition of PKA rescued the abnormal Runx2 and osteocalcin expression (Fig. 7G). Overall, these results suggest that elevated PKA signaling is responsible for microtia development and the transformation from chondrocytes to osteoblasts, consistent with the pro-osteogenic activity of PKA signaling.

Human microtia samples show increased PKA signaling and osteogenic differentiation

The above studies uncover a critical role for the BMP-PKA pathway in controlling auricle chondrocyte identity and microtia pathogenesis in mice. We also analyzed a single-cell RNA-seq dataset of the pinna of 2 microtia patients who may have disrupted *ROBO1/2* expression (Quiat et al., 2022) and detected a population of cells with osteoblast features besides chondrocytes, fibroblasts and endothelial cells (Supplementary Fig. S9A-C). Moreover, we found enriched gene expression in the PKA pathway, which was associated with *ADCY2* (Supplementary Fig. S9C-S9E). These results suggest a chondrocyte-to-osteoblast transformation under the influence of the PKA pathway in microtia patient samples. Although recent studies have uncovered an interaction between the BMP pathway and the Robo pathway (Morita et al., 2023; Tumelty et al., 2018), the functional link between these pathways in chondrocytes awaits further investigation.

Discussion

Microtia is usually a congenital disorder that affects the hearing and psychological health of affected children. Many of the disease candidate genes are involved in the proliferation and differentiation of auricle chondrocytes and therefore the development or growth of auricle cartilage (Gendron et al., 2016; Huang et al., 2023). Here, we show that in young or adult mice, ablation of *Bmpr1a* in auricle chondrocytes, which are genetically labelled by *Prrx1*, leads to rapid development of microtia. The function of BMP signaling in mature auricle chondrocytes appears to maintain cell identity and prevent chondrocytes from transforming into osteoblasts/osteoprogenitors. These results suggest that auricle appearance and integrity are actively maintained by BMP signaling.

Our study thus uncovered a novel function of BMP signaling in addition to its critical roles in chondrocyte proliferation and differentiation during endochondral ossification (Thielen et al., 2019). Defects in BMP-Smad1/5/9 signaling lead to achondroplasia and skeletal developmental defects. On the other hand, studies of *Bmpr1a* ablation mice using *Col1-CreERT*, *Prrx1-CreERT*, or *Dmp1-Cre* lines suggest that BMP-Smad1/5/9 signaling plays a modest pro-differentiation role in osteogenic lineage cells. Instead, BMP signaling in osteogenic lineage cells regulates osteoclastogenesis by affecting the relative expression of RANKL and OPG (He et al., 2017; Lim et al., 2016; Omi et al., 2019; Zhang et al., 2020). Here, we show that BMP signaling is required to maintain the cell fate of auricle chondrocytes by preventing them from osteogenic differentiation, thus expanding the physiological roles of BMP signaling in skeletal development and maintenance (Thielen et al., 2019).

Interestingly, we show that activation of BMP-Smad1/5/9 signaling in the auricle is uneven, with the distal part displaying the strongest activation in young or old mice. Accordingly, ablation of *Bmpr1a* in auricular chondrocytes mainly causes atrophy of the distal part. One possible explanation is that the distal part contains the most mature chondrocytes with the weakest regenerative ability. If so, it may mirror the trans-differentiation of terminally differentiated hypertrophic chondrocytes in the growth plate to osteoblasts (Tsang and Cheah, 2019). BMPs may be provided by chondrocytes themselves or by neighboring dermal cells, which warrants further investigation.

Our study suggests that the crosstalk between the BMP and PKA pathways plays a role in maintaining auricle chondrocyte fate. In the absence of *Bmpr1a*, the fate of chondrocytes is switched into osteoblast/osteoprogenitors, which can be blocked by PKA inhibition. Previous studies have shown that pharmacological inhibition of PKA efficiently blocks chondrogenic differentiation (Kozhemyakina et al., 2015). On the other hand, Sox9 inhibits chondrocyte hypertrophy and promotes the cell fate switch to osteoblasts/osteoprogenitors (Dy et al., 2012; Tsang and Cheah, 2019). This finding is consistent with a previous study showing that PKA promotes osteoblastogenesis and bone formation (Siddappa et al., 2008). How does BMP signaling regulate PKA activation? We found that the link is likely to be Adcy5/8, adenylate cyclases, whose expression is upregulated in the absence of BMP signaling. BMP signaling has been shown to suppress the expression of hepcidin and Robo4 (Morita et al., 2023; Wang et al., 2017). Since the Smad1/5/9 binding site in the promoters is very short, it may collaborate with other transcription factors to activate the transcription of target genes. In addition, BMP activates noncanonical signaling pathways, including MAPKs. As such, the underlying mechanisms for BMP-regulated expression of hepcidin, Robo4, Adcy5, and Adcy8 await further investigation (Morita et al., 2023; Wang et al., 2017).

Our findings may help to understand the pathogenesis of microtia in humans. A recent study uncovered a minimal microtia locus that carries a polymorphic repeat element, which may disrupt *ROBO1* and *ROBO2* gene expression in the auricle and be responsible for the high incidence of microtia in East Asian and Amerindian populations (Quiat et al., 2022). Analysis of the scRNA-seq data from microtia patients revealed that the microtia patient samples also showed enriched expression of osteoblast-related genes and the PKA pathway genes, suggesting that human microtia may share a pathogenesis similar to that in *Prrx1-CreERT; Bmpr1a*$^{f/f}$ mice, although this needs to be verified in the future.

In summary, this study shows that auricular chondrocytes can be genetically marked by Prrx1. Auricular chondrocytes, especially at the distal part of the ear, display BMP-Smd1/5/9 activation, which is required to maintain chondrocyte fate. In the

absence of BMP signaling, transformation of auricular chondrocytes into osteoblasts/osteoprogenitor cells will occur, leading to microtia development. This study thus deepens our understanding of microtia pathogenesis and expands the physiological functions of BMP-PKA crosstalk.

Materials and methods

Experimental design

The study was designed to examine the physiological function of BMP signaling in the maintenance of auricle chondrocyte and to elucidate the underlying molecular mechanisms.

Mouse maintenance

The knock-in *Prrx1-CreERT*^{2} mouse line was generated by Shanghai Biomodel Organism Science & Technology Development Co., Ltd. In this study, heterozygous *Prrx1-CreERT*^{2} mice were used for lineage tracing or gene ablation. *Rosa-tdTomato, Acta2-CreERT*^{2}, and *Col1α2-CreERT*^{2} mice were purchased from the Jackson Laboratory (https://www.jax.org/cn/). *Bmpr1a*$^{f/f}$ mice were generated in Yuji Mishina's laboratory. Animal experiments were carried out in accordance with recommendations in the National Research Council Guide for Care and Use of Laboratory Animals and in comply with relevant ethical regulations for animal testing and research, with the protocols approved by the Institutional Animal Care and Use Committee of Shanghai, China (SYXK(SH)2011-0112). This study follows the project that "Studies on the mechanism of MSC self-renewal differentiation and regulation of related tissue stem cells", which was approved by Shanghai Jiao Tong University in 2015 and the approval number is A2015027. Male mice were used in this study. Mice were anesthetized using 40 mg kg^{-1} sodium pentobarbital by intraperitoneal injection or euthanized by carbon dioxide inhalation.

Drug administration

Tamoxifen (Sigma) was dissolved in corn oil and administered peritoneally to mice at 120 mg kg^{-1} body weight daily for 3 days. For genetic tracing or gene ablation, mice were euthanized at different time points after tamoxifen (TAM).

For in vivo inhibition of PKA, H89 (Selleck Chemicals, USA) was dissolved in 5% DMSO, 40% PEG300, 5% Tween 80, and 50% ddH_2O at a final concentration of 1.05 mg/ml and was administered intraperitoneally every other day after tamoxifen injection. The dosage of H89 was 10 mg/kg (in 200 μl) each time. Mice were treated for 2 months

353 and then euthanized.

354 **Auricle regenerative experiments**

355 To investigate the regenerating ability of different parts of the mouse auricle, we drilled
356 a 2 mm (in diameter) hole at the distal, middle, or proximal parts of adult mice with a
357 uniform aperture. The mice were euthanized 1 month later, and the ear was analyzed to
358 assess the healing of the puncture wounds.

359 **RNA isolation and quantitative PCR**

360 Chondrocyte differentiation was also assessed with quantitative PCR. Total RNA
361 was extracted from the elastic cartilage using TRIzol reagent (Invitrogen), which was
362 reverse transcribed using the PrimerScriptTM RT reagent Kit (TaKaRa, RR037A) to
363 obtain cDNA. Quantitative PCR was performed using the Roche Light Cycler 480II
364 Assay system (Roche). The levels of different mRNA species were calculated with the
365 delta-delta CT method and normalized to *GAPDH*. The primer sequences are listed in
366 Supplementary Table S1.

367 **Immunohistochemistry and immunofluorescence staining**

368 The harvested ear tissues were fixed in 4% (vol/vol) neutral buffered formalin for
369 24 hours or directly embedded in optimal cutting temperature compound (OCT) by
370 liquid nitrogen without fixation. The harvested bone tissues were fixed in 4% (vol/vol)
371 neutral buffered formalin for 24 hours and decalcified in neutral 10% (wt/vol) EDTA
372 solution for 1 month at room temperature on the oscillator. For paraffin sectioning, the
373 samples were dehydrated, cleared, and embedded in paraffin blocks sequentially. The
374 paraffin-embedded tissues were cut at 10 μm with a paraffin microtome, and the frozen-
375 embedded tissues were cut at 8 μm with a cryostat. The ear tissue sections were
376 incubated overnight with anti-phospho-Smad1/5/9 antibody (Millipore, AB3848-1,
377 rabbit), anti-Ki67 antibody (Abcam, ab15580, rabbit), anti-Vimentin antibody (Abcam,
378 ab92547, rabbit), anti-αSMA antibody (Abcam, ab5694, rabbit), anti-Col1α1 antibody
379 (Abcam, ab21286, rabbit), anti-Col1α2 antibody (Santa Cruz, sc-393573, mouse), or
380 anti-phospho-CREB antibody (UPSTATE, 06-519, rabbit). The sections were then
381 incubated with goat anti-rabbit, mouse, or rat secondary antibodies conjugated with

Alexa Fluor 488 or 555 (Thermo Fisher Scientific). Slides were mounted with antifade mounting medium and DAPI (Thermo Fisher Scientific). Images were taken under an Olympus DP72 microscope (Olympus Microsystems).

H/E staining, ALP staining, and TUNEL staining

Paraffin sections were used for H/E staining and ALP staining with a commercial staining kit (TaKaRa, TRACP & ALP double-stain kit, Cat# MK300), while frozen sections were used for TUNEL staining with a kit (Roche, In Situ Cell Death Detection Kit, Fluorescein, REF11684795910).

Western blotting

Western blotting was performed with standard procedures. Proteins were extracted from the distal, mid, and proximal parts of the cartilage of the mouse ear using RIPA lysis buffer with 1 mM PMSF, 1 mg/ml pepstatin, leupeptin, and aprotonin. Samples were separated on 10% SDS–PAGE gels and transferred onto PVDF membranes (Millipore). Membranes were blocked with 5% milk or 3% BSA for 1 hr and incubated with specific antibodies overnight at 4 °C on a shaker. The primary antibodies included anti-phospho-Smad1/5/9 antibody (Millipore, AB3848-1, rabbit), anti-RUNX2 antibody (CST, 12556, rabbit), anti-RUNX2 antibody (CST, 12556, rabbit), anti-osteocalcin antibody (Abcam, ab93876, rabbit), anti-β−Actin antibody (Santa Cruz, sc47778, mouse), anti-phospho-CREB antibody (UPSTATE, 06-519, rabbit), or anti-CREB antibody (UPSTATE, 05-676, rabbit). The secondary antibodies included anti-rabbit IgG, HRP-linked antibody (CST, 7074, rabbit) and anti-mouse IgG, HRP-linked antibody (CST, 7076, mouse). The WB bands were visualized using the FluoChem M system (ProteinSimple). To quantify the western blotting results, we measured the density of each band by Image J, which was normalized to the loading control of the sample.

RNA sequencing

The distal part of the auricle of the mouse ear was harvested from control or knockout mice (n = 3 per group), from which RNA was isolated. RNA-seq was conducted by BGI Genomics Co., Ltd with the Illumina system. For data processing,

SOAP nuke (v1.5.2) was applied to filter reads and saved in FASTQ format. After quality control, clean reads were aligned to the reference mouse genome using Bowtie2 (v2.2.5) with default parameters. Gene expression levels were calculated and blasted with HISAT (v2.0.4) based on the Burrows–Wheeler transform and Ferragina-Manzini. Clean reads were then detected in terms of randomicity, coverage and degree of saturation. Statistically significant (adjusted p value ≤ 0.01) genes with large expression changes (fold change ≥ 1.5) were defined as differentially expressed genes. In pathway analysis and Gene Ontology (GO) analysis, all candidate genes were assorted according to official classification with the KEGG or GO annotation result, and phyper (a function of R) was performed for GO and pathway functional enrichment. Furthermore, GO analysis of the stage-specific gene signature was performed in the biological process category. The p value calculating formula was used based on wiki (https://en.wikipedia.org/wiki/Hypergeometric_distribution), and the false discovery rate (FDR) was calculated for each p value with FDR ≤ 0.01 defined as significantly enriched.

Statistical analysis

All measurements were collected by two authors who were blinded to the allocations of the mice. Image-Pro Plus was used to measure elastic cartilage thickness, cell volume, and ear size. GraphPad Prism 9.5.0 software was used to analyze and plot the ear thickness, cell volume, ear size, qPCR data, and immunofluorescence results. All quantitative data are presented as the means ± SD unless indicated otherwise. One-way ANOVA (and nonparametric or mixed) and two-way ANOVA (or mixed model) for multiple comparisons and unpaired two-tailed Student's t test were applied to evaluate the correlation data, and $p<0.05$ was considered statistically significant. We ensure that we have not set criteria and exclusions in this study. For each analysis, we reported the exact value of *n* in each experimental group.

Declarations

Acknowledgments

We thank Shoutao Qiu and Yuping Li for their technical assistance.

Funding

The work as supported by the National Key Research and Development Program of China (2018YFA0800803) and National Natural Science Foundation of China (92268101 and 32230045).

Availability of Data and Materials

The mouse auricle bulk RNA-seq data of *Prrx1-CreERT; Bmpr1a*$^{f/f}$ and control mice have been deposited into NCBI (GSE240126). Human scRNA-seq data of auricle samples (GSE202441) were analyzed. All other data generated or analyzed during this study are included in this published article and its additional files.

Author contributions

B. L., Z. Z., and H. L. designed the experiments, R. Y., H. C., and H. Y. performed the experiments, R. Y. and H. C. prepared the figures, Y. M. provided reagents, B. L., Z. Z., and H. L. wrote the paper. All authors read and approved the final manuscript

Declaration of interests

The authors declare no competing interests.

Data Availability

All data generated or analyzed in this study are included in this article, and are available from the corresponding author on request.

Reference

Abarca-Buis, R.F., and Krotzsch, E. (2023). Proximal ear hole injury heals by limited regeneration during the early postnatal phase in mice. J Anat *242*, 402-416.

Akiyama, H., Chaboissier, M.C., Martin, J.F., Schedl, A., and de Crombrugghe, B. (2002). The transcription factor Sox9 has essential roles in successive steps of the chondrocyte differentiation pathway and is required for expression of Sox5 and Sox6. Genes Dev *16*, 2813-2828.

Anthwal, N., and Thompson, H. (2016). The development of the mammalian outer and middle ear. J Anat *228*, 217-232.

Bielajew, B.J., Hu, J.C., and Athanasiou, K.A. (2020). Collagen: quantification, biomechanics, and role of minor subtypes in cartilage. Nat Rev Mater *5*, 730-747.

Chen, H., Tan, X.N., Hu, S., Liu, R.Q., Peng, L.H., Li, Y.M., and Wu, P. (2021). Molecular Mechanisms of Chondrocyte Proliferation and Differentiation. Front Cell Dev Biol *9*, 664168.

Cox, T.C., Camci, E.D., Vora, S., Luquetti, D.V., and Turner, E.E. (2014). The genetics of auricular development and malformation: new findings in model systems driving future directions for microtia research. Eur J Med Genet *57*, 394-401.

DiDomenico, C.D., Lintz, M., and Bonassar, L.J. (2018). Molecular transport in articular cartilage - what have we learned from the past 50 years? Nat Rev Rheumatol *14*, 393-403.

Dy, P., Wang, W., Bhattaram, P., Wang, Q., Wang, L., Ballock, R.T., and Lefebvre, V. (2012). Sox9 directs hypertrophic maturation and blocks osteoblast differentiation of growth plate chondrocytes. Dev Cell *22*, 597-609.

Evenbratt, H., Andreasson, L., Bicknell, V., Brittberg, M., Mobini, R., and Simonsson, S. (2022). Insights into the present and future of cartilage regeneration and joint repair. Cell Regen *11*, 3.

Fuchs, J.C., and Tucker, A.S. (2015). Development and Integration of the Ear. Curr Top Dev Biol *115*, 213-232.

Gendron, C., Schwentker, A., and van Aalst, J.A. (2016). Genetic Advances in the Understanding of Microtia. J Pediatr Genet *5*, 189-197.

Haseeb, A., Kc, R., Angelozzi, M., de Charleroy, C., Rux, D., Tower, R.J., Yao, L., Pellegrino da Silva, R., Pacifici, M., Qin, L*., et al.* (2021). SOX9 keeps growth plates and articular cartilage healthy by inhibiting chondrocyte dedifferentiation/osteoblastic redifferentiation. Proc Natl Acad Sci U S A *118*.

He, G., Shi, Y., Lim, J., Bellido, T., Ni, J., and Long, F. (2017). Differential involvement of Wnt signaling in Bmp regulation of cancellous versus periosteal bone growth. Bone Res *5*, 17016.

Huang, W., Zhou, X., Lefebvre, V., and de Crombrugghe, B. (2000). Phosphorylation of SOX9 by cyclic AMP-dependent protein kinase A enhances SOX9's ability to transactivate a Col2a1 chondrocyte-specific enhancer. Mol Cell Biol *20*, 4149-4158.

Huang, Y., Huang, X., Li, K., and Yang, Q. (2023). Risk Factors of Isolated Microtia: A Systematic Review and Meta-Analysis. Plast Reconstr Surg *151*, 651e-663e.

Jing, Y., Jing, J., Ye, L., Liu, X., Harris, S.E., Hinton, R.J., and Feng, J.Q. (2017). Chondrogenesis and osteogenesis are one continuous developmental and lineage defined biological process. Sci Rep *7*, 10020.

Kobayashi, S., Takebe, T., Inui, M., Iwai, S., Kan, H., Zheng, Y.W., Maegawa, J., and Taniguchi, H. (2011). Reconstruction of human elastic cartilage by a CD44+ CD90+ stem cell in the ear perichondrium. Proc Natl Acad Sci U S A *108*, 14479-14484.

501 Kozhemyakina, E., Lassar, A.B., and Zelzer, E. (2015). A pathway to bone: signaling molecules and
502 transcription factors involved in chondrocyte development and maturation. Development *142*,
503 817-831.
504 Lefebvre, V., Angelozzi, M., and Haseeb, A. (2019). SOX9 in cartilage development and disease.
505 Curr Opin Cell Biol *61*, 39-47.
506 Lim, J., Shi, Y., Karner, C.M., Lee, S.Y., Lee, W.C., He, G., and Long, F. (2016). Dual function of Bmpr1a
507 signaling in restricting preosteoblast proliferation and stimulating osteoblast activity in mouse.
508 Development *143*, 339-347.
509 Liu, C.F., Samsa, W.E., Zhou, G., and Lefebvre, V. (2017). Transcriptional control of chondrocyte
510 specification and differentiation. Semin Cell Dev Biol *62*, 34-49.
511 Liu, H., Li, P., Zhang, S., Xiang, J., Yang, R., Liu, J., Shafiquzzaman, M., Biswas, S., Wei, Z., Zhang, Z.*,*
512 *et al.* (2022). Prrx1 marks stem cells for bone, white adipose tissue and dermis in adult mice. Nat
513 Genet *54*, 1946-1958.
514 Lu, M., Lu, X., Jiang, H., and Pan, B. (2020). Review of Preferential Suspicious Genes in Microtia
515 Patients Through Various Approaches. J Craniofac Surg *31*, 538-541.
516 Mizuhashi, K., Ono, W., Matsushita, Y., Sakagami, N., Takahashi, A., Saunders, T.L., Nagasawa, T.,
517 Kronenberg, H.M., and Ono, N. (2018). Resting zone of the growth plate houses a unique class of
518 skeletal stem cells. Nature *563*, 254-258.
519 Morita, M., Yoneda, A., Tokunoh, N., Masaki, T., Shirakura, K., Kinoshita, M., Hashimoto, R.,
520 Shigesada, N., Takahashi, J., Tachibana, M.*, et al.* (2023). Upregulation of Robo4 expression by
521 SMAD signaling suppresses vascular permeability and mortality in endotoxemia and COVID-19
522 models. Proc Natl Acad Sci U S A *120*, e2213317120.
523 Murtaugh, L.C., Chyung, J.H., and Lassar, A.B. (1999). Sonic hedgehog promotes somitic
524 chondrogenesis by altering the cellular response to BMP signaling. Genes Dev *13*, 225-237.
525 Newton, P.T., Li, L., Zhou, B., Schweingruber, C., Hovorakova, M., Xie, M., Sun, X., Sandhow, L.,
526 Artemov, A.V., Ivashkin, E.*, et al.* (2019). A radical switch in clonality reveals a stem cell niche in the
527 epiphyseal growth plate. Nature *567*, 234-238.
528 Nordberg, R.C., Otarola, G.A., Wang, D., Hu, J.C., and Athanasiou, K.A. (2022). Navigating
529 regulatory pathways for translation of biologic cartilage repair products. Sci Transl Med *14*,
530 eabp8163.
531 Omi, M., Kaartinen, V., and Mishina, Y. (2019). Activin A receptor type 1-mediated BMP signaling
532 regulates RANKL-induced osteoclastogenesis via canonical SMAD-signaling pathway. J Biol Chem
533 *294*, 17818-17836.
534 Quiat, D., Kim, S.W., Zhang, Q., Morton, S.U., Pereira, A.C., DePalma, S.R., Willcox, J.A.L.,
535 McDonough, B., DeLaughter, D.M., Gorham, J.M.*, et al.* (2022). An ancient founder mutation
536 located between ROBO1 and ROBO2 is responsible for increased microtia risk in Amerindigenous
537 populations. Proc Natl Acad Sci U S A *119*, e2203928119.
538 Retting, K.N., Song, B., Yoon, B.S., and Lyons, K.M. (2009). BMP canonical Smad signaling through
539 Smad1 and Smad5 is required for endochondral bone formation. Development *136*, 1093-1104.
540 Ritter, K.E., and Martin, D.M. (2019). Neural crest contributions to the ear: Implications for
541 congenital hearing disorders. Hear Res *376*, 22-32.
542 Siddappa, R., Martens, A., Doorn, J., Leusink, A., Olivo, C., Licht, R., van Rijn, L., Gaspar, C., Fodde,
543 R., Janssen, F.*, et al.* (2008). cAMP/PKA pathway activation in human mesenchymal stem cells in

544 vitro results in robust bone formation in vivo. Proc Natl Acad Sci U S A *105*, 7281-7286.
545 Takarada, T., Hinoi, E., Nakazato, R., Ochi, H., Xu, C., Tsuchikane, A., Takeda, S., Karsenty, G., Abe,
546 T., Kiyonari, H., *et al.* (2013). An analysis of skeletal development in osteoblast-specific and
547 chondrocyte-specific runt-related transcription factor-2 (Runx2) knockout mice. J Bone Miner Res
548 *28*, 2064-2069.
549 ten Berge, D., Brouwer, A., Korving, J., Martin, J.F., and Meijlink, F. (1998). Prx1 and Prx2 in
550 skeletogenesis: roles in the craniofacial region, inner ear and limbs. Development *125*, 3831-3842.
551 Thielen, N.G.M., van der Kraan, P.M., and van Caam, A.P.M. (2019). TGFbeta/BMP Signaling
552 Pathway in Cartilage Homeostasis. Cells *8*.
553 Tsang, K.Y., and Cheah, K.S. (2019). The extended chondrocyte lineage: implications for skeletal
554 homeostasis and disorders. Curr Opin Cell Biol *61*, 132-140.
555 Tumelty, K.E., Higginson-Scott, N., Fan, X., Bajaj, P., Knowlton, K.M., Shamashkin, M., Coyle, A.J., Lu,
556 W., and Berasi, S.P. (2018). Identification of direct negative cross-talk between the SLIT2 and bone
557 morphogenetic protein-Gremlin signaling pathways. J Biol Chem *293*, 3039-3055.
558 Ueharu, H., and Mishina, Y. (2023). BMP signaling during craniofacial development: new insights
559 into pathological mechanisms leading to craniofacial anomalies. Front Physiol *14*, 1170511.
560 Wang, C.Y., Core, A.B., Canali, S., Zumbrennen-Bullough, K.B., Ozer, S., Umans, L., Zwijsen, A., and
561 Babitt, J.L. (2017). Smad1/5 is required for erythropoietin-mediated suppression of hepcidin in
562 mice. Blood *130*, 73-83.
563 Xie, Y., Zinkle, A., Chen, L., and Mohammadi, M. (2020). Fibroblast growth factor signalling in
564 osteoarthritis and cartilage repair. Nat Rev Rheumatol *16*, 547-564.
565 Yang, G., Zhu, L., Hou, N., Lan, Y., Wu, X.M., Zhou, B., Teng, Y., and Yang, X. (2014a). Osteogenic
566 fate of hypertrophic chondrocytes. Cell Res *24*, 1266-1269.
567 Yang, L., Tsang, K.Y., Tang, H.C., Chan, D., and Cheah, K.S. (2014b). Hypertrophic chondrocytes can
568 become osteoblasts and osteocytes in endochondral bone formation. Proc Natl Acad Sci U S A
569 *111*, 12097-12102.
570 Yoon, B.S., Ovchinnikov, D.A., Yoshii, I., Mishina, Y., Behringer, R.R., and Lyons, K.M. (2005). Bmpr1a
571 and Bmpr1b have overlapping functions and are essential for chondrogenesis in vivo. Proc Natl
572 Acad Sci U S A *102*, 5062-5067.
573 Yoon, B.S., Pogue, R., Ovchinnikov, D.A., Yoshii, I., Mishina, Y., Behringer, R.R., and Lyons, K.M.
574 (2006). BMPs regulate multiple aspects of growth-plate chondrogenesis through opposing actions
575 on FGF pathways. Development *133*, 4667-4678.
576 Zhang, H., Zhang, Y., Terajima, M., Romanowicz, G., Liu, Y., Omi, M., Bigelow, E., Joiner, D.M.,
577 Waldorff, E.I., Zhu, P., *et al.* (2020). Loss of BMP signaling mediated by BMPR1A in osteoblasts
578 leads to differential bone phenotypes in mice depending on anatomical location of the bones.
579 Bone *137*, 115402.

580

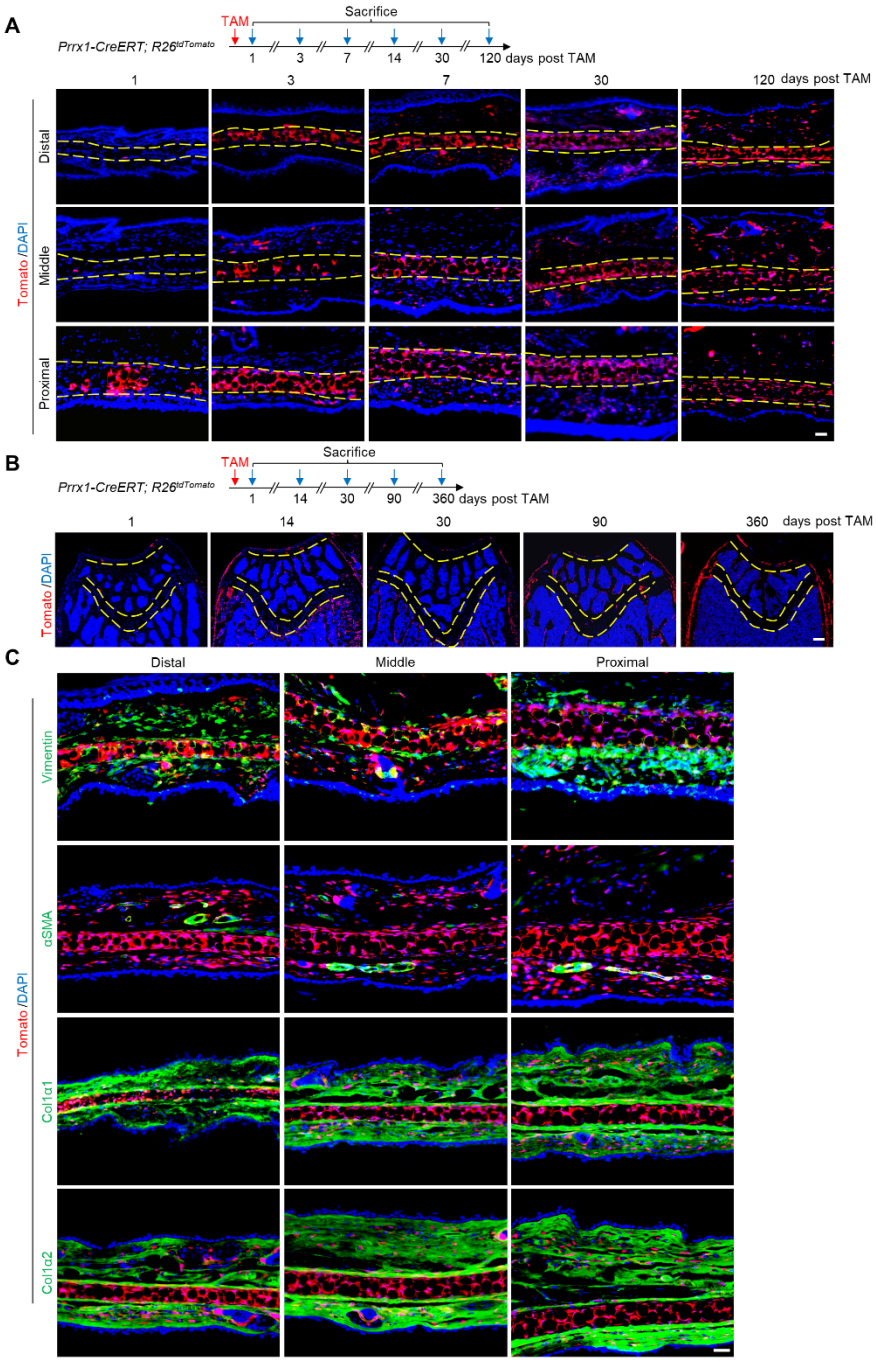

Figure 1. *Prrx1* marks auricle chondrocytes but few epiphyseal or articular chondrocytes.

A. Genetic tracing experiments showed that *Prrx1* marks all chondrocytes in the auricle. Upper panel: a diagram showing the schedule for TAM administration and mouse euthanasia. Scale bars=50 μm.

B. Genetic tracing experiments showed that Prrx1 marks few cells in growth plates or the articular cartilage of femurs in adult mice. Scale bars=50 μm.

C. Representative immunostaining results for Vimentin, αSMA, Col1α1, and Col1α2 in ear sections of *Prrx1-CreERT; R26^{tdTomato}* mice. Scale bars=50 μm.

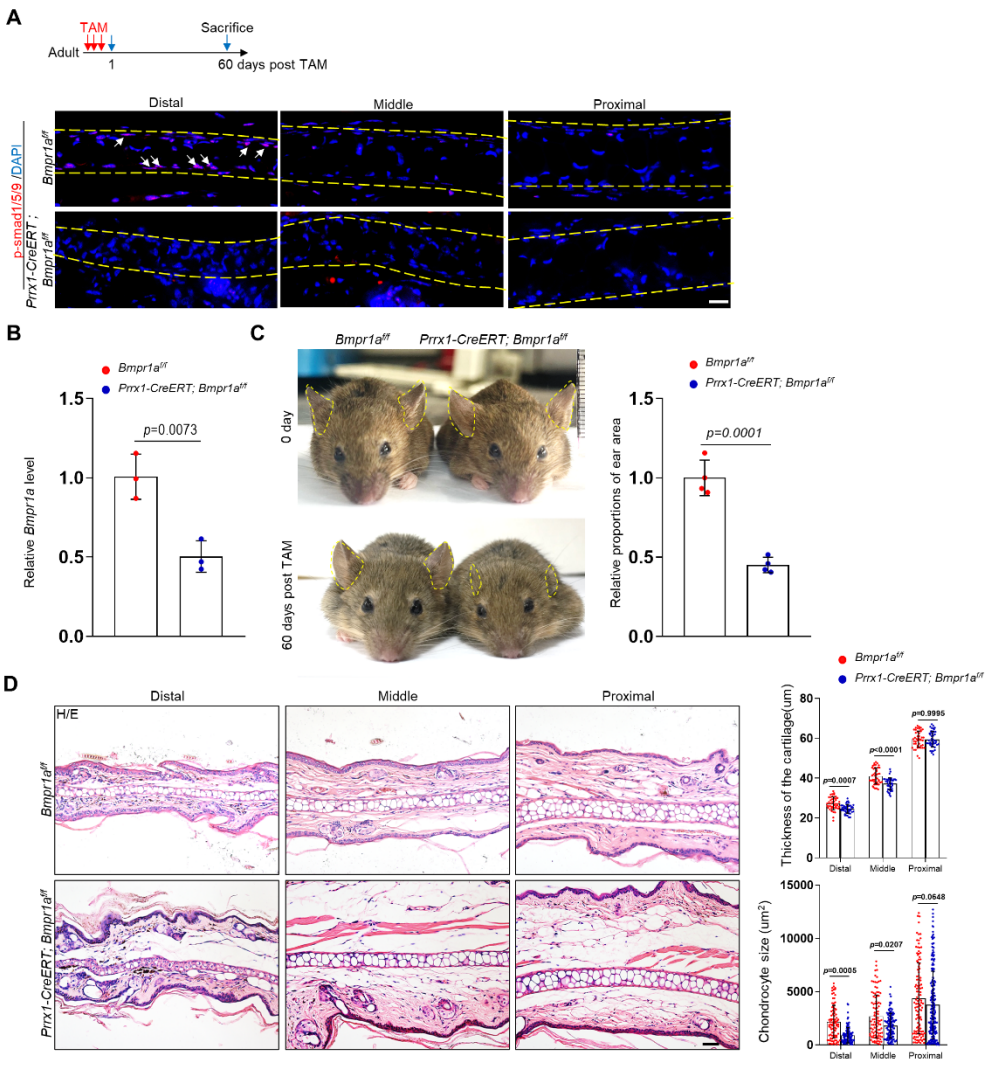

Figure 2

Figure 2. Ablation of *Bmpr1a* in *Prrx1*$^{+}$ cells in adult mice led to microtia.

A. A decrease in p-Smad1/5/9 on the ear sections of the *Prrx1-CreERT; Bmpr1a*$^{f/f}$ mice. Upper panel: Schedule for TAM administration and mouse euthanasia. Scale bars=20 μm. Arrows: positive signals.

B. qPCR analysis of *Bmpr1a* mRNA in the ear samples of the *Prrx1-CreERT; Bmpr1a*$^{f/f}$ and control mice. N=3.

C. The ear phenotypes of the *Prrx1-CreERT; Bmpr1a*$^{f/f}$ mice 2 months after TAM administration to adult male mice. Right panel: quantitation data. N=4.

D. H/E staining of ear sections from the mutant and control mice. Right panels: The thickness of the cartilage and the size of the chondrocytes in the ears of the mutant and control mice. Scale bars=50 μm. N=3. Unpaired two-tailed Student's t test were applied to evaluate the correlation data in (B and C). Two-way ANOVA (or mixed model) multiple comparisons were applied to evaluate the correlation data in (D), $p<0.05$ was considered as statistically significant.

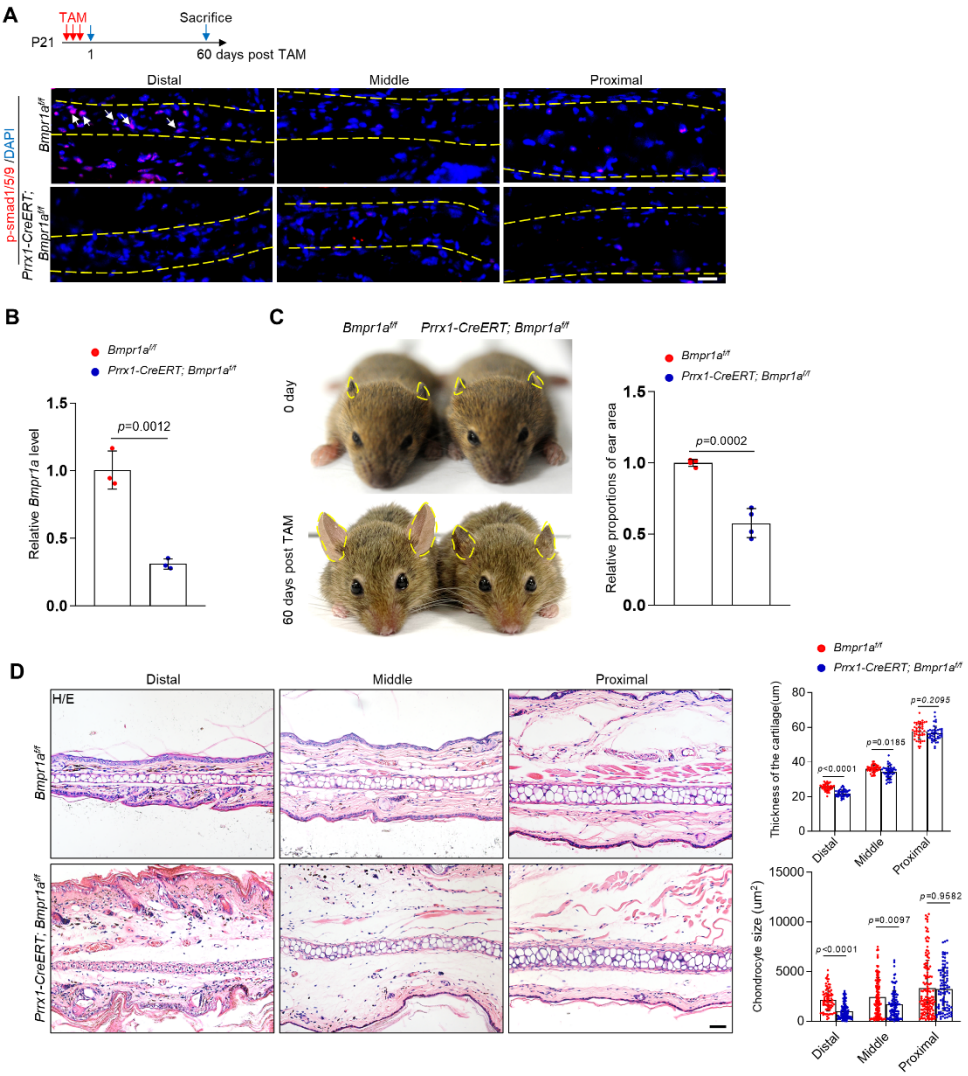

Figure 3

Figure 3. Ablation of *Bmpr1a* in *Prrx1*$^{+}$ cells in young mice led to microtia.

A. A decrease in p-Smad1/5/9 on the ear sections of the *Prrx1-CreERT; Bmpr1a*$^{f/f}$ mice that received TAM at P21. Upper panel: Schedule for TAM administration and mouse euthanasia. Scale bars=20 μm. Arrows: positive signals.

B. qPCR analysis of *Bmpr1a* mRNA in the ear samples of the *Prrx1-CreERT; Bmpr1a*$^{f/f}$ and control mice. N=3.

C. The ear phenotypes of the adult *Prrx1-CreERT; Bmpr1a*$^{f/f}$ mice that received Tam at P21. Right panel: quantitation data. N=4.

D. H/E staining of ear sections from the mutant and control mice. Right panels: The thickness of the cartilage and the size of the chondrocytes in the ears of the mutant and control mice. Scale bars=50 μm. N=3. Unpaired two-tailed Student's t test were applied to evaluate the correlation data in (B and C). Two-way ANOVA (or mixed model) multiple comparisons were applied to evaluate the correlation data in (D), $p<0.05$ was considered as statistically significant.

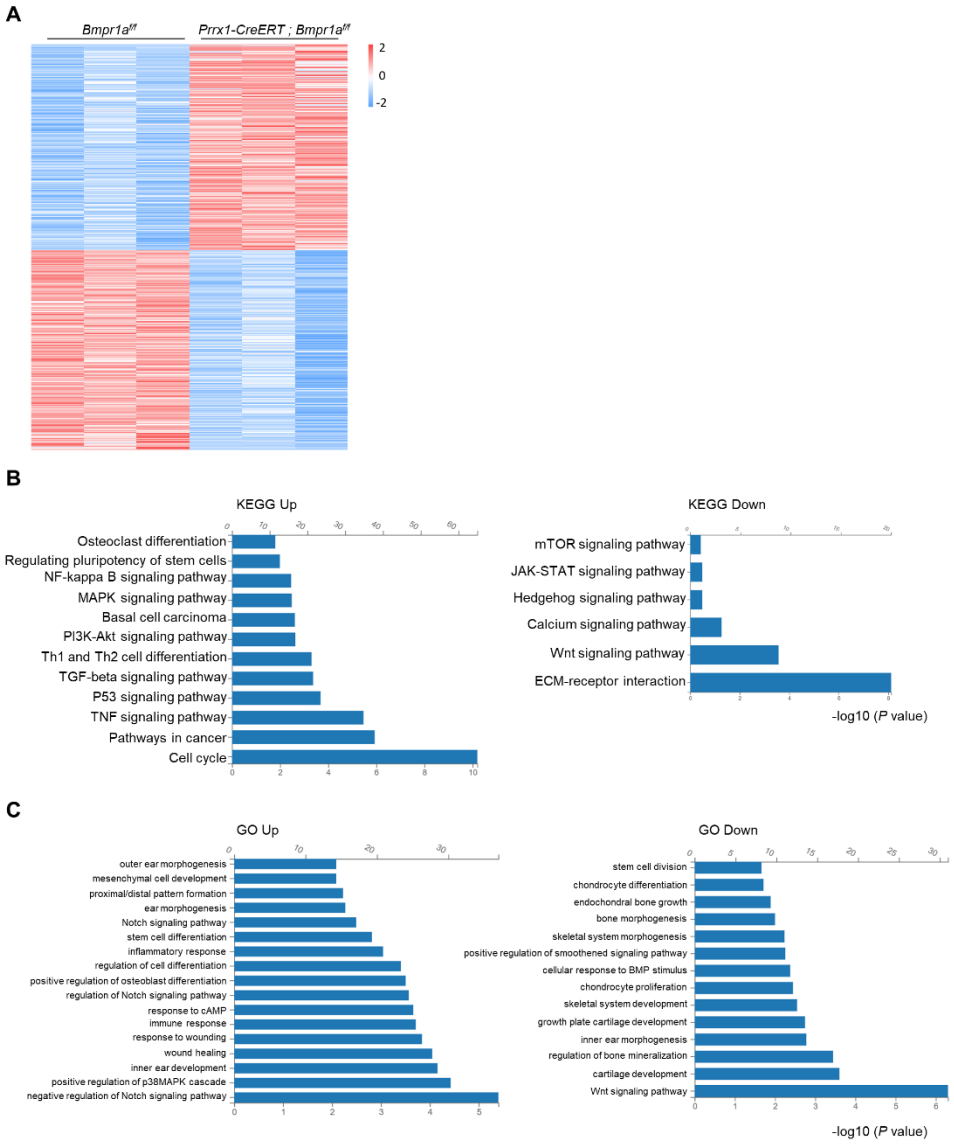

Figure 4

Figure 4. Alteration of transcription profiles in *Bmpr1a*-deficient chondrocytes.
A. Heatmaps of the top 500 genes expressed in the distal part of the auricle of the *Prrx1-CreERT; Bmpr1a*$^{f/f}$ and age- and gender-matched control mice. N=3.
B. KEGG analysis results of the pathways affected by *Bmpr1a* ablation.
C. GO analysis results of the modules affected by *Bmpr1a* ablation.

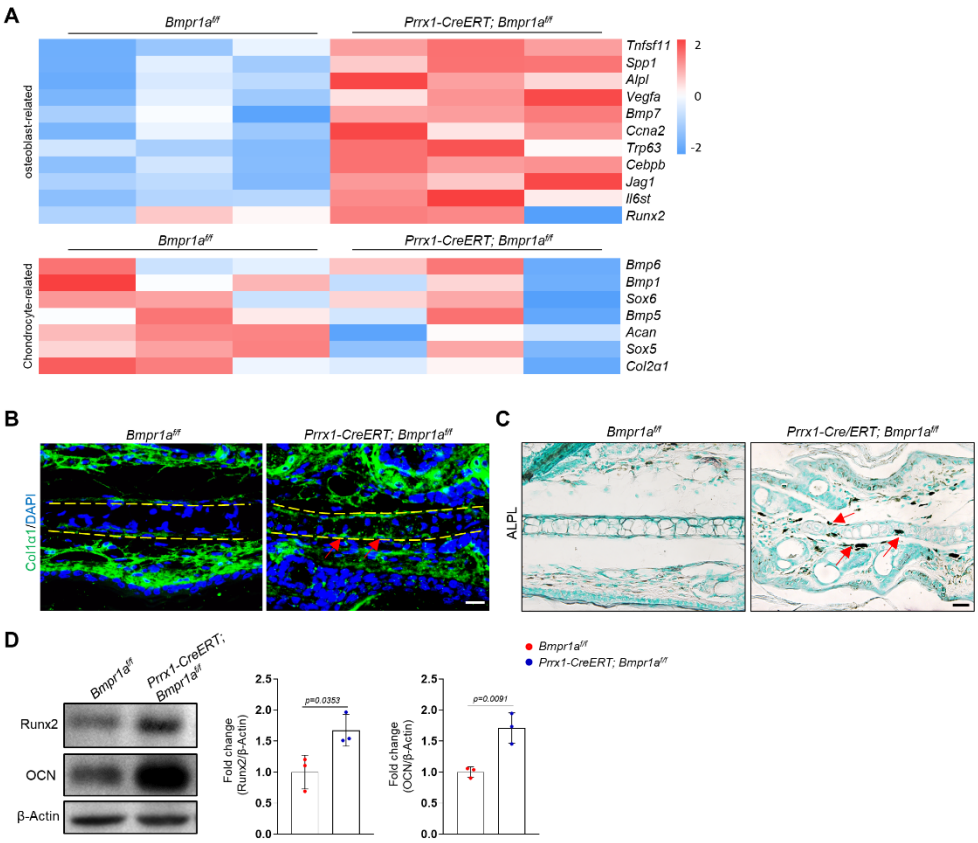

Figure 5

Figure 5. *Bmpr1a* deficiency leads to an auricle chondrocyte fate switch to osteoblasts.

A. Heatmaps of osteoblast-related genes and chondrocyte-related genes differentially expressed in the *Bmpr1a*-deficient and control mice. N=3.

B. Immunostaining results for Col1α1 in ear sections of the *Bmpr1a*-deficient and control mice. Scale bars=20 μm. Arrows: positive signals.

C. ALP activity was greatly increased in the auricle of the *Prrx1-CreERT; Bmpr1a*$^{f/f}$ mice compared to the control mice. Scale bars=50 μm. Arrows: positive signals.

D. WB results showed that the expression of the osteoblast marker genes Runx2 and osteocalcin was increased in the mutant samples. Right panel: quantitation data. N=3. Unpaired two-tailed Student's t test were applied to evaluate the correlation data in (D), $p<0.05$ was considered as statistically significant.

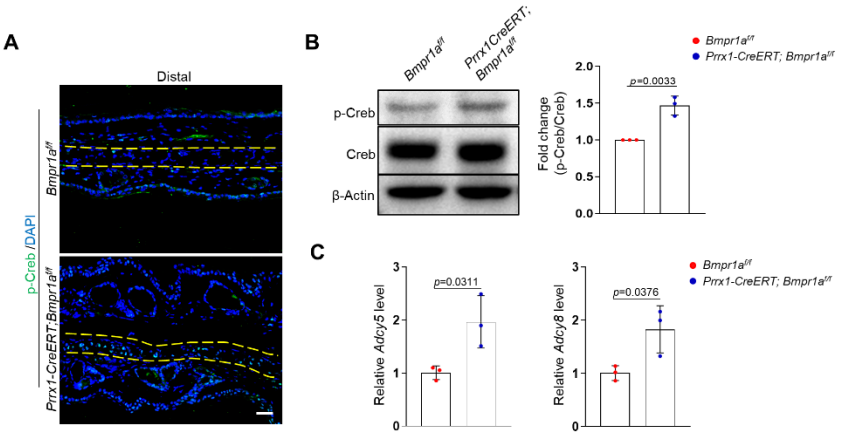

Figure 6

Figure 6. *Bmpr1a* deficiency led to hyperactivation of PKA signaling.
A. Immunoassaying for p-Creb in the ear sections of the *Bmpr1a*-deficient and control mice.
B. Western blot analysis of p-Creb in auricle samples of the *Bmpr1a*-deficient and control mice. Right panel: quantitation data. N=3.
C. qPCR results for *Adcy5* and *Adcy8* in auricle samples of the *Bmpr1a*-deficient and control mice. N=3. Unpaired two-tailed Student's t test were applied to evaluate the correlation data in (B and C), $p<0.05$ was considered as statistically significant.

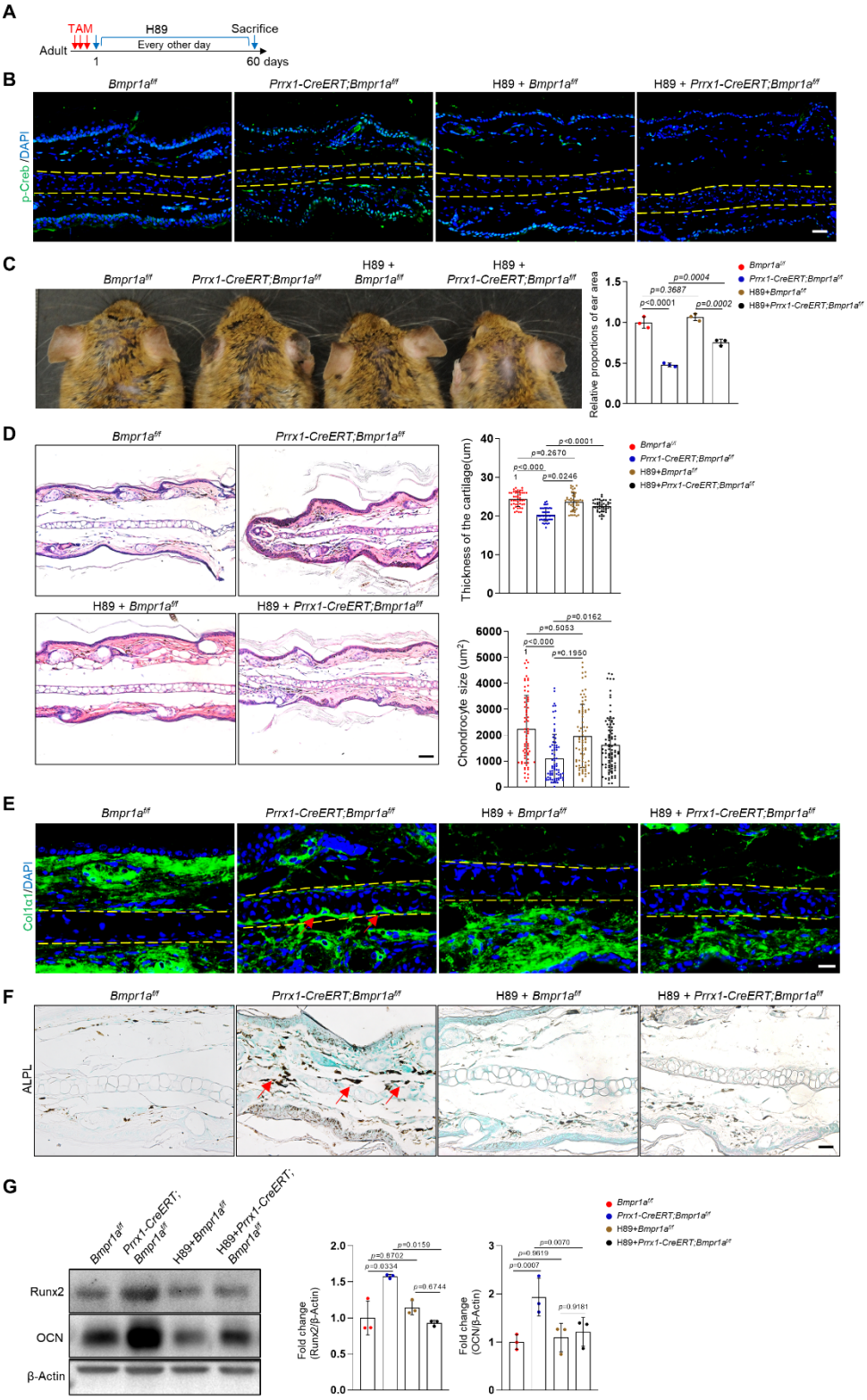

Figure 7

Figure 7. Inhibition of PKA signaling blocks microtia development in *Bmpr1a*-deficient mice

A. Diagram showing the schedule of TAM and H89 administration.

B. Immunostaining results of p-Creb in ear sections of the H89-treated mutant and control mice. Scale bars=50 μm.

C. The rescue of the microtia phenotype in the mutant mice by H89. Right panels: Quantitation data. N=3.

D. H/E staining results. Right panels: the thickness of the cartilage and the size of the chondrocytes in the ear of the mutant and control mice. N=3. Right panels: Quantitation data. Scale bars=50 μm. N=3.

E. Immunostaining results for Col1α1 in the ear sections of the H89-treated mutant and control mice. Scale bars=20 μm. Arrows: positive signals.

F. ALP activity was greatly suppressed by H89 in the auricle of the *Prrx1-CreERT; Bmpr1a*$^{f/f}$ mice compared to the control mice. Scale bars=50 μm. Arrows: positive signals.

G. WB blot also showed that H89 rescued the expression of the osteoblast marker genes Runx2 and osteocalcin in the mutant mice. Right panel: quantitation data. N=3. One-way ANOVA (and nonparametric or mixed) multiple comparisons were applied to evaluate the correlation data in (C, D, and G). $p<0.05$ was considered as statistically significant.